Ab Initio Computation of Charge Densities for Sn and Xe Isotopes

P. Arthuis[1,*] C. Barbieri[1,2,3,†] M. Vorabbi[4,‡] and P. Finelli[5,§]

[1]Department of Physics, University of Surrey, Guildford GU2 7XH, United Kingdom
[2]Dipartimento di Fisica, Università degli Studi di Milano, Via Celoria 16, I-20133 Milano, Italy
[3]INFN, Sezione di Milano, Via Celoria 16, I-20133 Milano, Italy
[4]National Nuclear Data Center, Bldg. 817, Brookhaven National Laboratory, Upton, New York 11973-5000, USA
[5]Dipartimento di Fisica e Astronomia, Università degli Studi di Bologna and INFN,
Sezione di Bologna, Via Irnerio 46, I-40126 Bologna, Italy

We present the first *ab initio* calculations for open-shell nuclei past the tin isotopic line, focusing on Xe isotopes as well as doubly magic Sn isotopes. We show that, even for moderately hard interactions, it is possible to obtain meaningful predictions and that the $NNLO_{sat}$ chiral interaction predicts radii and charge density distributions close to the experiment. We then make a new prediction for ^{100}Sn. This paves the way for *ab initio* studies of exotic charge density distributions at the limit of the present *ab initio* mass domain, where experimental data is becoming available. The present study closes the gap between the largest isotopes reachable by *ab initio* methods and the smallest exotic nuclei accessible to electron scattering experiments.

Introduction.—The charge density distribution of the atomic nucleus offers a unique access to its internal structure and the spatial distribution of the nucleons. This distribution has been probed for decades using electron scattering experiments off stable isotopes [1–3] that have provided an impressive amount of accurate experimental data. Unfortunately, measurements on nuclei outside the valley of stability have been prevented by the difficulties associated with preparing short-lived targets despite the interest in studying exotic nuclei presenting features like neutron halos, neutron skins, or proton bubbles [4–8]. Such investigations have recently been made possible with the construction of the self-confining radioactive-isotope ion target (SCRIT) at RIKEN [9–11] and will be explored as well in the next few years at the Facility for Antiproton and Ion Research by the European Learning and Intelligent Systems Excellence project [12]. By successfully using an electron storage ring as a trap for the radioactive ions, the SCRIT experimenters have been able to scatter electrons off ^{132}Xe nuclei and recently published their first results [11]. While other isotopes in the $A \sim 130$ mass region will be studied over the next years, experimental luminosities might prevent studying lighter nuclei before future upgrades, limiting charge distribution extraction from exotic nuclei to the heavy mass sector.

A flourishing of new or reimplemented formalisms [13–25] associated with new numerical approaches [26–28] have allowed *ab initio* methods to finally leave the realm of light nuclei and access midmass isotopes up to $A \sim 100$ [29,30] over the past few decades. But all of those approaches seem to have reached a new ceiling with the Sn isotopic line. The limitations preventing them from reaching higher masses are diverse—from interactions based on chiral effective field theory overbinding midmass nuclei [31,32] to numerical limitations linked to the size of the basis and the matrix elements storage.

Recently, new interactions have been developed [33–37] leading to an improvement in the reproduction of experimental data for midmass nuclei. New frameworks have been proposed for the treatment of both the Hamiltonian and the many-body formalism [38–41], paving the way toward larger model spaces and promising to extend the reach of *ab initio* methods within the next few years. While a first qualitative reproduction of Sn closed-shell nuclei ground-state energies had been obtained a few years ago [29], the spectroscopy of the light end of the Sn isotopic chain has only been investigated recently [30] with an interaction able to reproduce experimental results for heavier nuclei [33]. This raises the question of using present day frameworks to extend the frontier of the *ab initio* domain and compare results from calculations to experimental charge distributions that will become available at SCRIT. Investigating discrepancies between *ab initio* theoretical predictions and experimental results will allow one to put new constraints on the experiment, inform our theoretical models, and open the way to the study of heavy nuclei structure from first principles.

In this Letter, we use the self-consistent Green's function theory (SCGF) [13–15] with chiral effective field theory Hamiltonians, present what are to our knowledge the first *ab initio* calculations of charge radius, neutron skin, and charge density distributions for ^{100}Sn, ^{132}Sn, ^{132}Xe, ^{136}Xe,

and ^{138}Xe, and reproduce the experimental cross section obtained at SCRIT for ^{132}Xe.

Self-consistent Green's function theory.—For solving the A-body Schrödinger equation, SCGF theory [13,15] expresses the nucleon dynamics in terms of one- to A-body propagators or Green's functions. These propagators are expanded in perturbative series that are recast into the exact Green's functions within a self-consistent scheme, implicitly resumming infinite sets of diagrams. The one-body propagators are particularly interesting as they give access to all one-body observables and to the ground-state energy through the Galitskii–Migdal–Koltun sum rule [42]. A unique and interesting feature of the one-body propagator is that it also gives access to information on the neighboring nuclei [43,44].

In order to obtain the one-body Green's function, one solves the intrinsically nonperturbative Dyson equation, which relies on the irreducible self-energy encoding all nontrivial many-body correlations between individual nucleons and the nuclear medium. In particular, this comprises both information on the A-nucleon ground state and scattering states of the $A + 1$ systems, making SCGF a natural *ab initio* approach for computing structure and reaction observables consistently [45,46]. To be able to access open-shell nuclei, where pairing has to be included for a qualitatively correct description, Dyson SCGFs have been generalized using a $U(1)$-symmetry-breaking reference state obtained from solving the Hartree–Fock–Bogoliubov equation, yielding the Gorkov SCGF theory [14]. While the broken particle-number symmetry has to be restored eventually, such a development remains to be formulated for Gorkov SCGF.

In this Letter, the self-energy is obtained via the algebraic diagrammatic construction approach, or ADC(n) [47,48], which comprises all perturbative contributions up to order n plus any infinite order resummation that is needed to preserve the spectral representation. At the moment, the Dyson SCGF has been numerically implemented up to ADC(3) [43,48], but the Gorkov formalism has only been implemented up to ADC(2) [31], such that the following calculations made on open-shell nuclei are done at the ADC (2) level. Both truncation levels incorporate mean-field as well as $2p1h$ and $2h1p$ contributions. While the two-body force is treated fully, the three-body force is included in the final calculation in an effective way, as described in [42,43].

Results.—For the present work, we will mostly focus on the NNLO$_{\mathrm{sat}}$ [34] Hamiltonian as it offers one of the best reproductions of radii and densities for medium-mass nuclei among chiral interactions [36]. This interaction is used bare and incorporates both two-body forces and three-body forces at the next-to-next-to-leading order (NNLO) in the chiral development. We performed calculations in a spherical harmonic oscillator basis, with frequencies ranging from $\hbar\Omega = 10$ to 16 MeV, where the minimum for the ground-state energy was shown to reside by a first set of
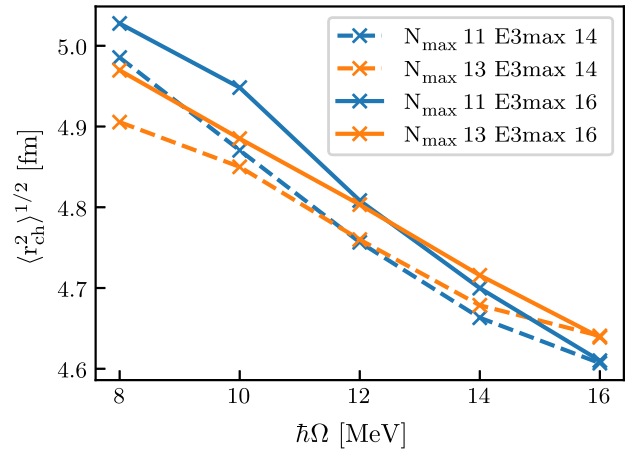

FIG. 1. Model space dependence of the charge radius for ^{132}Xe obtained from Gorkov SCGF calculations at ADC(2).

exploratory calculations. All the states of the single-particle basis up to $N_{\mathrm{max}} = 13$ are used, i.e., 14 major shells and one- and two-body operators are fully included. This is, however, not feasible for three-body operators due to the exponential increase in the number of their matrix elements and the associated storage cost. Consequently, only three-body excitations up to $E_{3\,\mathrm{max}} = 16$ were considered. The restricted size of the single-particle basis and the cut on the number of three-body matrix elements prevented us from obtaining converged results for the ground-state energy, as previously observed with NNLO$_{\mathrm{sat}}$ on ^{78}Ni [49]. As such, we do not discuss such results in this Letter.

Let us first study the case of ^{132}Xe. Figure 1 provides the value of the charge radius for ^{132}Xe obtained from Gorkov SCGF calculations at the ADC(2) truncation level over a range of harmonic oscillator frequencies that includes the optimal value. The solid (dashed) lines indicate calculations using three-body matrix elements for triplet excitations up to $E_{3\,\mathrm{max}} = 16$ ($E_{3\,\mathrm{max}} = 14$), while the orange (blue) lines correspond to a model space of $N_{\mathrm{max}} = 13$ ($N_{\mathrm{max}} = 11$). The expected behavior, i.e., a decrease in the radius with larger frequencies and the radius becoming independent of the frequency with larger model spaces, is reproduced. Given that the converged value of the charge radius is expected to be near the crossing of the $N_{\mathrm{max}} = 13$ and 11 lines [50–52], we choose here and for the other nuclei to take a conservative estimate [53] by considering that it lies between the highest value at $\hbar\Omega = 10$ MeV and the lowest one at 14 MeV. As can be seen here and consistently with what is obtained for the other nuclei, the cut on the three-body matrix element has only a limited effect on the value of the charge radius. Though they are not shown here, similar results have been obtained with the other nuclei discussed in the following.

In addition to the convergence in terms of model space and number of three-body matrix elements, the convergence in terms of the truncation scheme must be

considered. Among the nuclei studied in this Letter, only ^{100}Sn and ^{132}Sn are doubly magic and can be computed at the ADC(3) truncation level. Our investigations show that, as observed previously on lighter nuclei [8,36,56], the difference between the ADC(2) and ADC(3) values for the charge radius (and similarly for the charge density distribution) is very small, such that it is basically converged at the ADC(2) level. As such, we do not discuss differences between ADC(2) and ADC(3) results any further in this Letter. In the following, we will hence represent our results as a band obtained for frequencies from 10 to 14 MeV at $N_{max} = 13$ and from 12 to 14 MeV at $N_{max} = 11$ for $E_{3\,max} = 16$.

From this procedure, the charge radius of ^{132}Xe is estimated to be 4.824 ± 0.124 fm, which agrees with the value recently extracted from the SCRIT experiment of $\langle r^2 \rangle^{1/2} = 4.79^{+0.11}_{-0.08}$ fm [10]. For comparison, the calculations have been reproduced using the newly proposed $NN + 3N(\mathrm{lnl})$ interaction [36], which is known to have good convergence properties with respect to the model space size and to give results similar to the very successful 1.8/2.0(EM) interaction [33]. In contrast to NNLO$_{\mathrm{sat}}$, the charge radius obtained for ^{132}Xe is 4.070 ± 0.045 fm, largely underestimating the experimental value consistently with studies on lighter nuclei [36]. Despite this failure at reproducing the experimental value of the charge radius, one notices that values obtained from $NN + 3N(\mathrm{lnl})$ converge better than for NNLO$_{\mathrm{sat}}$, as expected from the softness of $NN + 3N(\mathrm{lnl})$. This relative hardness of NNLO$_{\mathrm{sat}}$, tied to the nonlocal cutoff on the three-body terms, has been shown to play an important role for saturation properties of nuclear matter [57] and thus helps for a good reproduction of both energies and radii, in contrast to $NN + 3N(\mathrm{lnl})$.

In addition to the sole charge radius, another quantity that can be computed from SCGF calculations is the charge density distribution. In the case of ^{132}Xe, the SCRIT group extracted the constants c and t for a two-parameter Fermi charge distribution $\rho(r) = \rho_0 / \{1 + \exp[4 \ln 3(r - c)/t]\}$. Figure 2 displays this two-point Fermi distribution as a dotted line with a gray band representing the error bars, while the green band represents our SCGF calculations. It can be observed that while the SCGF calculations agree with the two-point Fermi distribution at the surface of the nucleus, though slightly overpredicting the charge radius, we obtain an oscillating behavior for the density inside the nucleus that cannot be reproduced with only a two-point Fermi distribution. Extracting a three-point Fermi distribution from the experiment would require an increase in its luminosity such that possible discrepancies between theory and experiment cannot be discussed any further here.

To better gauge the discrepancies between the theoretical and experimental bands in Fig. 2, we compare the computed electron scattering cross sections directly to
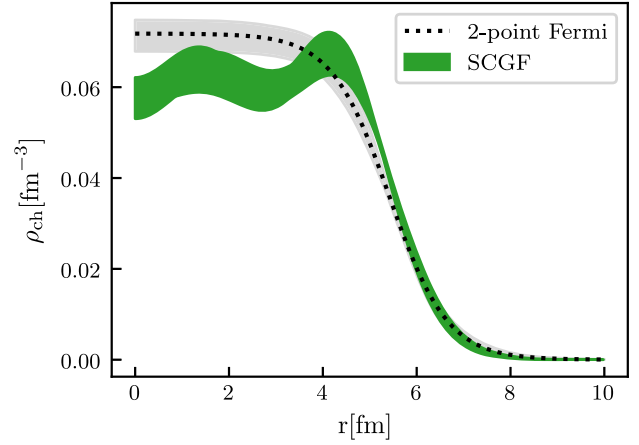

FIG. 2. Charge density distribution for ^{132}Xe obtained from Gorkov SCGF calculations at ADC(2). The dotted line with gray band corresponds to the two-point Fermi distribution with parameter and error bars extracted from Ref. [10].

SCRIT data. Figure 3 displays the differential cross sections multiplied by the luminosity as a function of the effective momentum transfer for the three experimental electron beam energies of $E_e = 151$ MeV, 201 MeV, and
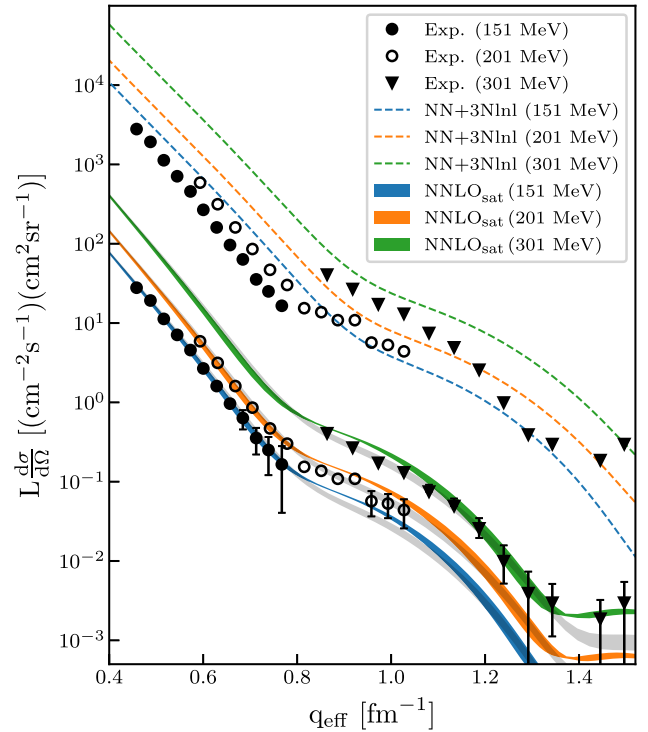

FIG. 3. Luminosity multiplied by the differential cross section for ^{132}Xe obtained from Gorkov SCGF calculations at ADC(2). The values for the $NN + 3N(\mathrm{lnl})$ interaction have been scaled by 10^2 for clarity. The gray bands correspond to the two-point Fermi distribution with parameter and error bars extracted from Ref. [10]. Experimental values are taken from [10] and duplicated with a scaling of 10^2 for comparison with $NN + 3N(\mathrm{lnl})$ values, where error bars have been removed for clarity.

301 MeV. The experimental points and error bars are taken from Ref. [10]. The different bands are computed using the DREPHA code [58] starting from the nuclear charge density distributions obtained from the two-point Fermi distribution of Ref. [10] (gray bands) and from our SCGF calculations using $NNLO_{sat}$ (colored bands). The calculation is performed in the distorted wave Born approximation [59–61]. The results show very good agreement with the experimental values, with only an interval of effective momentum transfers between 0.8 fm^{-1} and 1.1 fm^{-1} being slightly off the error bars. To discard the density oscillations within the nucleus as the source of the discrepancy, we fitted a two-point Fermi density to the radius and surface predicted by the theory. Calculations using this Fermi distribution gave results within the band obtained from the genuine SCGF density. This confirms the inability of the experiment to give insights on the internal structure of the nucleus without going past the second minimum in the cross section. As a comparison, the results obtained with the $NN + 3N(lnl)$ interaction are displayed as well, scaled upward for clarity. Contrary to $NNLO_{sat}$, the $NN + 3N(lnl)$ interaction fails at reproducing the experimental values, as expected with an underestimated charge radius. This demonstrates the unique capacity of $NNLO_{sat}$ to reproduce radii and density distributions and sets an important precedent in the use of SCGF with the $NNLO_{sat}$ interaction for pre- or postdiction of experimental results from electron scattering off exotic nuclei. In particular, this motivates experimental measurements at higher momentum transfer to properly gauge the internal structure of nuclei.

Having proved the capacity of SCGF and $NNLO_{sat}$ to give meaningful insights on the charge radius and density distributions of ^{132}Xe, charge densities have also been calculated for ^{100}Sn, ^{132}Sn, ^{136}Xe, and ^{138}Xe for this Hamiltonian. These are displayed in Fig. 4. The behavior
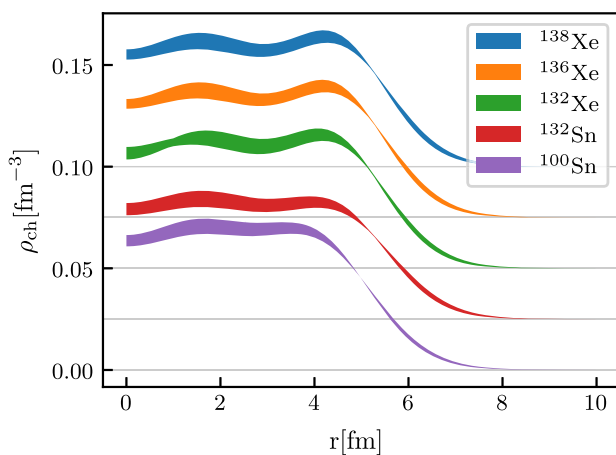

FIG. 4. Charge density distributions for ^{100}Sn, ^{132}Sn, ^{132}Xe, ^{136}Xe, and ^{138}Xe obtained from Gorkov SCGF calculations. The charge density is shifted upward by 0.025 fm^{-3} between each two nuclei, and the colored bands indicate the theoretical error associated with model space convergence.

TABLE I. Charge radii in fm obtained from SCGF calculations and $NNLO_{sat}$ compared to experimental values from Ref. [62].

	SCGF	Experiment
^{100}Sn	4.525–4.707	
^{132}Sn	4.725–4.956	4.709 3
^{132}Xe	4.700–4.948	4.785 9
^{136}Xe	4.715–4.928	4.796 4
^{138}Xe	4.724–4.941	4.827 9

of the charge distributions is qualitatively similar for all of them, with oscillations of the density within the nucleus and the possibility of a slight depletion at its center.

The charge radii extracted from our calculations are displayed for the same Sn and Xe isotopes in Table I and compared to the experimental results [62]. Our results show overall a good reproduction of the experimental data and are a proof of the capacity of $NNLO_{sat}$ to produce accurate results in the heavy nuclei regime, even despite the inability to obtain converged values for the ground-state energy. In the future, more accurate calculations with smaller errors may uncover slight differences between $NNLO_{sat}$ and the experimental values. Among the nuclei studied, ^{100}Sn stands out as a particularly interesting case. ^{100}Sn sits close to the proton dripline [63] at the end of superallowed α-decay chains [64,65], has the largest strength known in allowed β decay [66], and is expected to be the heaviest doubly magic nucleus with $N = Z$ [67]. Despite of these properties, experimental data in its area are scarce [68]; in particular, neither its spectrum nor its radius have been measured yet. While its spectrum has recently been predicted from first principles [30], Table I displays the first *ab initio* prediction of its charge radius.

Neutron skins are directly related to the density dependence of the nuclear symmetry energy, a quantity critical to the determination of the nuclear equation of state and associated astrophysical properties [69]. SCGF calculations in the mass range $A = 40$–64 [36] suggest that $NNLO_{sat}$ and $NN + 3N(lnl)$ yield nearly identical skins in spite of their differences in the prediction of radii [70]. These neutron skins tend to be systematically higher (or smaller proton skins) than the experimental findings from Ref. [71] but are within the reported error bars. Our results for Sn and Xe are shown in Table II for both Hamiltonians. Although

TABLE II. Neutron skins in fm computed with SCGF. Each interval indicates the theoretical error associated with model space convergence.

	$NNLO_{sat}$	$NN + 3N(lnl)$
^{100}Sn	−0.079 to −0.096	−0.060 to −0.068
^{132}Sn	0.168 to 0.197	0.180 to 0.275
^{132}Xe	0.103 to 0.128	0.120 to 0.152
^{136}Xe	0.128 to 0.156	0.134 to 0.223
^{138}Xe	0.143 to 0.175	0.152 to 0.251

they are consistent with each other within the uncertainties from the model space convergence, $NN + 3N(\text{lnl})$ gives slightly higher values. These differences correlate with the differences in charge radii found in Ref. [72]. For ^{132}Sn, neutron skins of 0.24(4) fm [73] and 0.258(24) fm [74] have been extracted from measurements of low-lying dipole excitations, while Skyrme functionals predict 0.263–0.294 fm [75]. The NNLO$_{\text{sat}}$ is in disagreement with these values, as can be expected, since it is already known to miss the expected symmetry energy at saturation density [76]. These results stress the need for accurate experimental data in the neutron-rich areas of the nuclear chart, where *ab initio* calculations tend to struggle to reproduce radii [77].

Conclusions.—Our calculations demonstrate the capacity of SCGF and the NNLO$_{\text{sat}}$ interaction to give a meaningful estimation of the charge radius and charge density distribution of heavy nuclei up to mass $A = 138$, which had never been studied before. We computed successfully the charge radius, density distribution, and neutron skins of ^{132}Sn, ^{132}Xe, ^{136}Xe, and ^{138}Xe, mostly agreeing with known experimental values, and gave the first *ab initio* prediction for the charge radius and density distribution of ^{100}Sn. In particular, we reproduced the experimental cross section of the SCRIT electron scattering experiment for ^{132}Xe, demonstrating the capacity of *ab initio* methods with well-designed chiral interactions to be used for the internal structure study of heavy exotic nuclei, alongside new experimental facilities. Our error bars, though conservative, are small enough to shed light on discrepancies with experimental values, informing theory and putting constraints on experiments. In particular, our results are a motivation for measurements at higher momentum transfer to probe the internal structure of the nuclei.

[*]parthuis@theorie.ikp.physik.tu-darmstadt.de
[†]carlo.barbieri@unimi.it
[‡]mvorabbi@bnl.gov
[§]paolo.finelli@bo.infn.it

[1] B. Hahn, D. G. Ravenhall, and R. Hofstadter, Phys. Rev. 101, 1131 (1956).
[2] R. Hofstadter, Rev. Mod. Phys. 28, 214 (1956).
[3] S. Boffi, C. Giusti, and F. Pacati, Phys. Rep. 226, 1 (1993).
[4] E. Khan, M. Grasso, J. Margueron, and N. V. Giai, Nucl. Phys. A800, 37 (2008).
[5] M. Grasso, L. Gaudefroy, E. Khan, T. Nikšić, J. Piekarewicz, O. Sorlin, N. Van Giai, and D. Vretenar, Phys. Rev. C 79, 034318 (2009).
[6] I. Tanihata, H. Savajols, and R. Kanungo, Prog. Part. Nucl. Phys. 68, 215 (2013).
[7] Z.-J. Wang, Z.-Z. Ren, and T.-K. Dong, Chin. Phys. C 38, 024102 (2014).
[8] T. Duguet, V. Somà, S. Lecluse, C. Barbieri, and P. Navrátil, Phys. Rev. C 95, 034319 (2017).
[9] T. Suda, T. Adachi, T. Amagai, A. Enokizono, M. Hara, T. Hori, S. Ichikawa, K. Kurita, T. Miyamoto, R. Ogawara, T. Ohnishi, Y. Shimakura, T. Tamae, M. Togasaki, M. Wakasugi, S. Wang, and K. Yanagi, Prog. Theor. Exp. Phys. 2012, 03C008 (2012).
[10] K. Tsukada, A. Enokizono, T. Ohnishi, K. Adachi, T. Fujita, M. Hara, M. Hori, T. Hori, S. Ichikawa, K. Kurita, K. Matsuda, T. Suda, T. Tamae, M. Togasaki, M. Wakasugi, M. Watanabe, and K. Yamada, Phys. Rev. Lett. 118, 262501 (2017).
[11] K. Tsukada *et al.*, Proc. Sci., INPC2016 (2017) 007.
[12] A. N. Antonov *et al.*, Nucl. Instrum. Methods Phys. Res., Sect. A 637, 60 (2011).
[13] W. H. Dickhoff and C. Barbieri, Prog. Part. Nucl. Phys. 52, 377 (2004).
[14] V. Somà, T. Duguet, and C. Barbieri, Phys. Rev. C 84, 064317 (2011).
[15] C. Barbieri and A. Carbone, Lect. Notes Phys. 936, 571 (2017).
[16] K. Kowalski, D. J. Dean, M. Hjorth-Jensen, T. Papenbrock, and P. Piecuch, Phys. Rev. Lett. 92, 132501 (2004).
[17] P. Piecuch, J. R. Gour, and M. Włoch, Int. J. Quantum Chem. 109, 3268 (2009).
[18] G. Hagen, T. Papenbrock, D. J. Dean, and M. Hjorth-Jensen, Phys. Rev. C 82, 034330 (2010).
[19] K. Tsukiyama, S. K. Bogner, and A. Schwenk, Phys. Rev. Lett. 106, 222502 (2011).
[20] H. Hergert, S. K. Bogner, T. D. Morris, A. Schwenk, and K. Tsukiyama, Phys. Rep. 621, 165 (2016).
[21] E. Gebrerufael, K. Vobig, H. Hergert, and R. Roth, Phys. Rev. Lett. 118, 152503 (2017).
[22] A. Tichai, E. Gebrerufael, K. Vobig, and R. Roth, Phys. Lett. B 786, 448 (2018).
[23] A. Tichai, P. Arthuis, T. Duguet, H. Hergert, V. Somá, and R. Roth, Phys. Lett. B 786, 195 (2018).
[24] P. Demol, T. Duguet, A. Ekström, M. Frosini, K. Hebeler, S. König, D. Lee, A. Schwenk, V. Somà, and A. Tichai, Phys. Rev. C 101, 041302(R) (2020).
[25] S. R. Stroberg, S. K. Bogner, H. Hergert, and J. D. Holt, Annu. Rev. Nucl. Part. Sci. 69, 307 (2019).
[26] S. K. Bogner, R. J. Furnstahl, and R. J. Perry, Phys. Rev. C 75, 061001(R) (2007).
[27] S. K. Bogner, R. J. Furnstahl, and A. Schwenk, Prog. Part. Nucl. Phys. 65, 94 (2010).
[28] R. J. Furnstahl and K. Hebeler, Rep. Prog. Phys. 76, 126301 (2013).

[29] S. Binder, J. Langhammer, A. Calci, and R. Roth, Phys. Lett. B **736**, 119 (2014).

[30] T. D. Morris, J. Simonis, S. R. Stroberg, C. Stumpf, G. Hagen, J. D. Holt, G. R. Jansen, T. Papenbrock, R. Roth, and A. Schwenk, Phys. Rev. Lett. **120**, 152503 (2018).

[31] V. Somà, A. Cipollone, C. Barbieri, P. Navrátil, and T. Duguet, Phys. Rev. C **89**, 061301(R) (2014).

[32] V. Lapoux, V. Somà, C. Barbieri, H. Hergert, J. D. Holt, and S. R. Stroberg, Phys. Rev. Lett. **117**, 052501 (2016).

[33] K. Hebeler, S. K. Bogner, R. J. Furnstahl, A. Nogga, and A. Schwenk, Phys. Rev. C **83**, 031301(R) (2011).

[34] A. Ekström, G. R. Jansen, K. A. Wendt, G. Hagen, T. Papenbrock, B. D. Carlsson, C. Forssén, M. Hjorth-Jensen, P. Navrátil, and W. Nazarewicz, Phys. Rev. C **91**, 051301(R) (2015).

[35] A. Ekström, G. Hagen, T. D. Morris, T. Papenbrock, and P. D. Schwartz, Phys. Rev. C **97**, 024332 (2018).

[36] V. Somà, P. Navrátil, F. Raimondi, C. Barbieri, and T. Duguet, Phys. Rev. C **101**, 014318 (2020).

[37] T. Hüther, K. Vobig, K. Hebeler, R. Machleidt, and R. Roth, Phys. Lett. B **808**, 135651 (2020).

[38] D. Frame, R. He, I. Ipsen, D. Lee, D. Lee, and E. Rrapaj, Phys. Rev. Lett. **121**, 032501 (2018).

[39] A. Tichai, R. Schutski, G. E. Scuseria, and T. Duguet, Phys. Rev. C **99**, 034320 (2019).

[40] A. Tichai, J. Ripoche, and T. Duguet, Eur. Phys. J. A **55**, 90 (2019).

[41] A. Ekström and G. Hagen, Phys. Rev. Lett. **123**, 252501 (2019).

[42] A. Carbone, A. Cipollone, C. Barbieri, A. Rios, and A. Polls, Phys. Rev. C **88**, 054326 (2013).

[43] A. Cipollone, C. Barbieri, and P. Navrátil, Phys. Rev. C **92**, 014306 (2015).

[44] V. Somà, Front. Phys. **8**, 340 (2020).

[45] S. J. Waldecker, C. Barbieri, and W. H. Dickhoff, Phys. Rev. C **84**, 034616 (2011).

[46] A. Idini, C. Barbieri, and P. Navrátil, Phys. Rev. Lett. **123**, 092501 (2019).

[47] J. Schirmer, L. S. Cederbaum, and O. Walter, Phys. Rev. A **28**, 1237 (1983).

[48] F. Raimondi and C. Barbieri, Phys. Rev. C **97**, 054308 (2018).

[49] G. Hagen, G. R. Jansen, and T. Papenbrock, Phys. Rev. Lett. **117**, 172501 (2016).

[50] A. Nogga, P. Navrátil, B. R. Barrett, and J. P. Vary, Phys. Rev. C **73**, 064002 (2006).

[51] S. Bogner, R. Furnstahl, P. Maris, R. Perry, A. Schwenk, and J. Vary, Nucl. Phys. **A801**, 21 (2008).

[52] A. Tichai, J. Müller, K. Vobig, and R. Roth, Phys. Rev. C **99**, 034321 (2019).

[53] The present calculations have been made using the value $\langle r_p^2 \rangle = 0.77$ fm^2 that was included in the CODATA compilation [54]. As a result of recent experiments, the CODATA value was updated to $\langle r_p^2 \rangle = 0.7079$ fm^2 [55].

As the deviation coming from using the old value was negligible with respect to our estimated uncertainties, we do not consider it further in this Letter.

[54] P. J. Mohr, B. N. Taylor, and D. B. Newell, Rev. Mod. Phys. **80**, 633 (2008).

[55] CODATA recommended values of the fundamental physical constants: 2018 (2018).

[56] C. Barbieri, N. Rocco, and V. Somà, Phys. Rev. C **100**, 062501(R) (2019).

[57] G. Hagen, T. Papenbrock, A. Ekström, K. A. Wendt, G. Baardsen, S. Gandolfi, M. Hjorth-Jensen, and C. J. Horowitz, Phys. Rev. C **89**, 014319 (2014).

[58] S. Klein, B. Dreher, and J. Friedrich, Drepha: A phase-shift calculation code for elastic electron scattering (1986).

[59] D. R. Yennie, D. G. Ravenhall, and R. N. Wilson, Phys. Rev. **95**, 500 (1954).

[60] H. Uberall, Electron Scattering from Complex Nuclei, *Pure and Applied Physics* (Academic Press, New York, 1971).

[61] C. C. degli Atti, Prog. Part. Nucl. Phys. **3**, 163 (1980).

[62] I. Angeli and K. Marinova, At. Data Nucl. Data Tables **99**, 69 (2013).

[63] J. Erler, N. Birge, M. Kortelainen, W. Nazarewicz, E. Olsen, A. M. Perhac, and M. Stoitsov, Nature (London) **486**, 509 (2012).

[64] S. N. Liddick *et al.*, Phys. Rev. Lett. **97**, 082501 (2006).

[65] D. Seweryniak, K. Starosta, C. N. Davids, S. Gros, A. A. Hecht, N. Hoteling, T. L. Khoo, K. Lagergren, G. Lotay, D. Peterson, A. Robinson, C. Vaman, W. B. Walters, P. J. Woods, and S. Zhu, Phys. Rev. C **73**, 061301(R) (2006).

[66] C. B. Hinke *et al.*, Nature (London) **486**, 341 (2012).

[67] M. Lewitowicz *et al.*, Phys. Lett. B **332**, 20 (1994).

[68] T. Faestermann, M. Górska, and H. Grawe, Prog. Part. Nucl. Phys. **69**, 85 (2013).

[69] M. Centelles, X. Roca-Maza, X. Viñas, and M. Warda, Phys. Rev. Lett. **102**, 122502 (2009), and references therein.

[70] V. Somà (private communication) (2020).

[71] A. Trzcińska, J. Jastrzębski, P. Lubiński, F. J. Hartmann, R. Schmidt, T. von Egidy, and B. Kłos, Phys. Rev. Lett. **87**, 082501 (2001).

[72] G. Hagen, A. Ekström, C. Forssén, G. R. Jansen, W. Nazarewicz, T. Papenbrock, K. A. Wendt, S. Bacca, N. Barnea, B. Carlsson, C. Drischler, K. Hebeler, M. Hjorth-Jensen, M. Miorelli, G. Orlandini, A. Schwenk, and J. Simonis, Nat. Phys. **12**, 186 (2016).

[73] A. Klimkiewicz *et al.* (LAND Collaboration), Phys. Rev. C **76**, 051603(R) (2007).

[74] A. Carbone, G. Colò, A. Bracco, L.-G. Cao, P. F. Bortignon, F. Camera, and O. Wieland, Phys. Rev. C **81**, 041301(R) (2010).

[75] S. Burrello, M. Colonna, G. Colò, D. Lacroix, X. Roca-Maza, G. Scamps, and H. Zheng, Phys. Rev. C **99**, 054314 (2019).

[76] A. Carbone, Phys. Rev. Research **2**, 023227 (2020).

[77] R. F. G. Ruiz *et al.*, Nat. Phys. **12**, 594 (2016).